A&A 386, 874–883 (2002)
DOI: 10.1051/0004-6361:20020210

Astronomy & Astrophysics

The 3 μm spectrum of R Doradus observed with the ISO-SWS*

N. Ryde[1] and K. Eriksson[2]

[1] Department of Astronomy, University of Texas, Austin, TX 78712-1083, USA
[2] Uppsala Astronomical Observatory, Box 515, 751 20 Uppsala, Sweden
e-mail: kjell.eriksson@astro.uu.se

Received 25 September 2001 / Accepted 31 January 2002

Abstract. We have modeled the 2.6–3.7 μm spectrum of the red semiregular variable R Doradus observed with the Short-Wavelength Spectrometer on board the Infrared Space Observatory. The wavelength resolution of the observations varies between $R \sim 2000$–2500. We have calculated a synthetic spectrum using a hydrostatic model photosphere in spherical geometry. The agreement between the synthetic spectrum and the ISO observations is encouraging, especially in the wavelength region of 2.8–3.7 μm, suggesting that a hydrostatic model photosphere is adequate for the calculation of synthetic spectra in the near infrared for this moderately varying red giant star. However, an additional absorption component is needed at 2.6–2.8 μm and this discrepancy is discussed. The spectral signatures are dominated by water vapour in the stellar photosphere, but several photospheric OH, CO, and SiO features are also present. The effective temperature and surface gravity derived for R Dor, based on the 2.6–3.7 μm ISO spectrum and the modeling of it with a hydrostatic model photosphere, are 3000 ± 100 K and $\log g = 0 \pm 1$ (cgs), respectively. The spectral region observed is found to be temperature sensitive. The effective temperature given here is slightly higher than those reported in the literature. We also discuss possible reasons for this.

Key words. stars: individual: R Dor – stars: AGB and post-AGB – stars: late-type – infrared: stars

1. Introduction

R Doradus is one of the brightest stars in the infrared. Its flux distribution peaks in the 1 μm range, the spectral type being M8III[1]. R Dor is classified as a semi-regular variable (SRb; Kholopov 1988), or more precisely a red SRV (for a definition, see Kerschbaum & Hron 1992), but is closely related to the Mira variables in the sense that it probably lies near the edge of a Mira instability strip (Bedding et al. 1997). R Dor has, however, a longer period than expected for SRVs, but this fact could be due to irregularities in the periods (Kerschbaum & Hron 1992) or could be telling us that SRVs with long periods represent a sub-group of Mira stars (Bedding et al. 1998).

Semi-regular variables are most likely evolved stars on the Asymptotic Giant Branch (AGB) in the HR diagram, see for example Habing (1996). AGB stars are low-initial-mass stars with electron-degenerate, carbon-oxygen cores on their way from the main sequence towards the white-dwarf/planetary-nebula phase. Approximately 95% of all stars will eventually pass this stage of evolution (Habing 1996). In general, there seems to be an evolutionary sequence on the AGB from the blue SRVs to the long-period Mira stars, passing through the red SRV phase (Kerschbaum & Hron 1992; Lebzelter & Hron 1999). The blue SRVs are supposed to be on the early AGB, the red SRVs are suggested to be experiencing the first thermal pulses, and finally the Miras are associated with the thermal pulses and are supposed to be pulsating in the fundamental mode, showing large amplitudes in the visual brightness.

A key feature of AGB stars is their massive but slow stellar winds, creating an extensive circumstellar envelope. AGB stars and their circumstellar envelopes in general present spherical symmetry (see for example Olofsson 1996). In combination with the thermal pulses and the subsequent third dredge-up, which drags up newly synthesised elements into the atmosphere, the wind causes an enrichment of the interstellar medium in elements synthesised in the AGB star, thus making these stars important actors in the chemical evolution of galaxies (see for example Gustafsson & Ryde 2000). R Dor has a mass-loss rate of $7 \times 10^{-8}\,M_{\odot}\,\mathrm{yr}^{-1}$, which is at the lower end of what is typical for AGB stars, and a wind velocity of

Send offprint requests to: N. Ryde,
e-mail: ryde@astro.as.utexas.edu

* Based on observations with ISO, an ESA project with instruments funded by ESA Member States (especially the PI countries: France, Germany, The Netherlands and the UK) and with the participation of ISAS and NASA. The SWS is a joint project of SRON and MPE.

[1] http://simbad.u-strasbg.fr/

6 km s^{-1} (Loup et al. 1993). R Dor shows some circumstellar dust emission (see discussions in Bedding et al. 1998; Kerschbaum & Hron 1992) and also molecular circumstellar emission from regions close to the star (see for example Ryde et al. 1999).

Thanks to the Infrared Space Observatory (ISO), launched in 1995, it has become possible to study the atmospheres of red giants in detail at low and medium resolution, also at wavelengths obscured by the Earth's atmosphere, for example the interesting region between the K- and L-bands studied here.

Here we present the 2.60–3.66 μm medium-resolution ($R \sim 2500$) spectrum of R Dor, observed by the ISO-SWS, and model it by generating a synthetic spectrum from the photosphere only. This results in a good agreement. The photosphere is modeled with the latest version of the MARCS model photosphere code, generating hydrostatic photospheres. The study of infrared (IR) spectra of red giants provides a test of the adequacy of hydrostatic model photospheres, their input data and their constraints, for the modeling of red giants.

In their unmasking of the warm molecular-envelopes surrounding AGB stars Tsuji et al. (1997) model the 3 μm spectrum of the M 6 giant g Her and the M 7 giant SW Vir observed by the Short-Wavelength Spectrometer (SWS) on board ISO. Markwick & Millar (2000) model the same wavelength region of ISO-SWS observations of the Mira star R Cas (M7III). They suggest that the absorption spectrum originates from the inner regions of the circumstellar envelope, and model it with two circumstellar components, one warm and one cold.

2. Observations

The spectrum of R Dor was observed with the SWS (de Graauw et al. 1996) on board ISO (Kessler et al. 1996). The spectrometer was used in the grating scan mode (SWS06), which provides a resolution of $R \sim 2000$–2500, depending on the wavelength in the observed region.

The 44 min of observations were performed on the 23rd June 1997 during ISO revolution number 585. The reductions were made using the pipeline, basic reduction package OLP (version 9.5) and the ISO Spectral Analysis Package (ISAP version 2.0). The pipeline processing of the data, such as the flux calibration, is described in the ISO-SWS Handbook. The accuracy of the calibration of the absolute flux is better than 7% (1σ).

We also observed a low-resolution spectrum from 2.4 μm to 45 μm of R Dor with the ISO-SWS (in the SWS01 mode) on 27th June 1997 (orbit number 589). Also here, the reductions were made using OLP version 9.5 and ISAP version 2.0. Our SWS06 and SWS01 spectra of R Dor were thus observed within 4 days of each other. The variation in the spectra due to the periodic variations in the star can therefore safely be ignored, R Dor having a period of 338 days (Kholopov 1988). The SWS01 observation, in the wavelength region of our SWS06 observation, is composed of two sub-spectra; bands 1B and 1D. These two sub-spectra could be merged into one spectrum directly.

Due to the way the spectrometer works in the SWS06 mode, our region was observed in five spectral bands: 2.60–3.02 μm, 3.02–3.08 μm, 3.08–3.19 μm, 3.19–3.50 μm, and 3.52–3.66 μm (for details, see the ISO Handbook de Graauw et al. 2000). There are mismatches in the fluxes between these bands due to uncertainties in the detector gains in every band. Furthermore, the overlap between the bands is small. Therefore, in order to align the five bands, we used the low-resolution SWS01 spectrum, convolved to $\Delta\lambda = 0.1\,\mu$m or a resolution of $R \sim 30$, to outline the spectral shape of the region we observed. In this way we are able to scale the different bands of the SWS06 observation with correct factors in order to merge the bands into one spectrum. The flux levels of the bands observed, lie within a factor of 1.04 of each other. As a check, after having merged the SWS06 sub-spectra, we also convolved the merged spectrum to $R \sim 30$, which resulted in the same shape as the SWS01 observation convolved to $R \sim 30$. This indicates that we were successful in merging the five sub-spectra into one spectrum over the entire region and that we can rely on the overall shape of the observed spectrum.

In Figs. 1 and 2 we show the observed ISO spectra. The resolution of the five bands are $R = 2300$, 2500, 2000, 2500, and 2000, respectively (de Graauw et al. 2000).

3. Model photospheres and the generation of synthetic spectra

For the purpose of analysing our observations, synthetic spectra have been generated (Ryde et al. 1998) using model photospheres from the new grid of spherically-symmetric model photospheres of M giants, which is currently being calculated with the latest version of the MARCS code. This version is the final major update (of the code and its input data) in the suite of MARCS model-photosphere programs first developed by Gustafsson et al. (1975) and further improved in several steps, e.g. by Plez et al. (1992), Jørgensen et al. (1992), and Edvardsson et al. (1993).

These hydrostatic, spherical model photospheres are computed on the assumptions of Local Thermodynamic Equilibrium (LTE), homogeneity and the conservation of the total flux (radiative plus convective; the convective flux being computed using the mixing length formulation). The radiative field used in the model generation, is calculated with absorption from atoms and molecules by opacity sampling in approximately 84 000 wavelength points over the entire, relevant wavelength range considered for the star (2300 Å–20 μm).

Data on the absorption by atomic species are collected from the VALD database (Piskunov et al. 1995) and Kurucz (1995, private communication). The opacity of CO, CN, CH, OH, NH, TiO, VO, ZrO, H_2O, FeH, CaH, C_2, MgH, SiH, and SiO are included and up-to-date dissociation energies and partition functions are used.

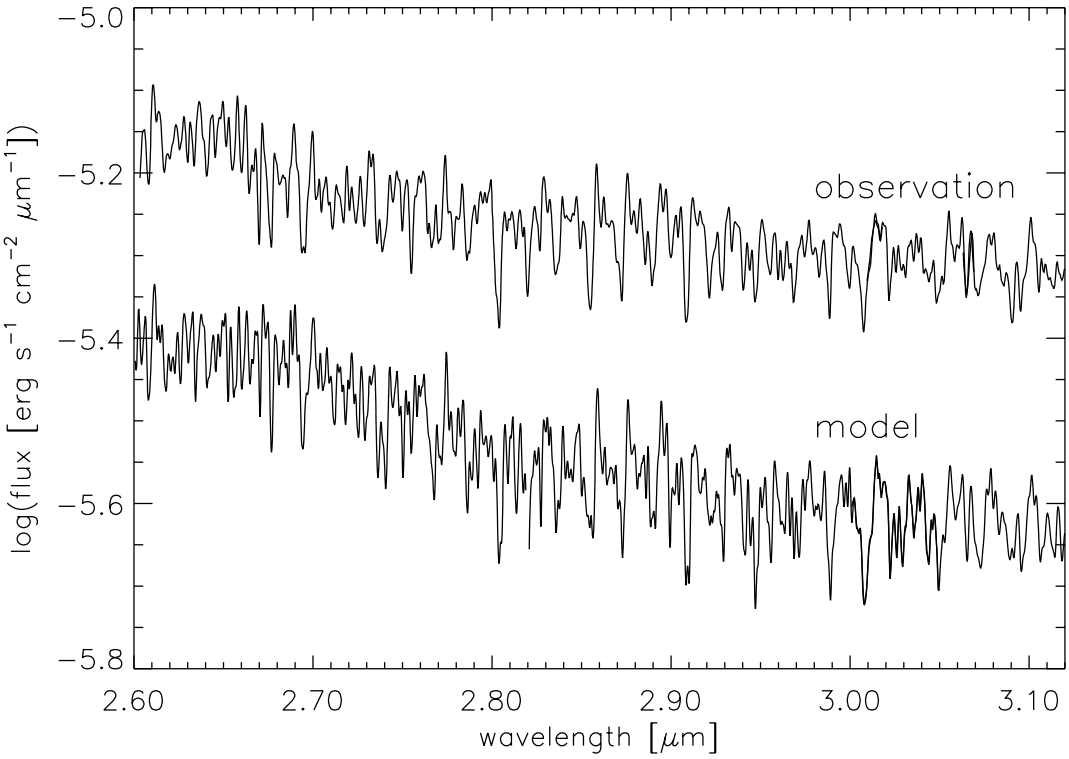

Fig. 1. The first half of the observed spectrum of R Dor is shown as the upper spectrum. The modeled spectrum, which is shifted down for clarity, is shown below. The modeled spectrum is convolved with a Gaussian whose width matches the appropriate resolution of the bands observed. The abscissa scale shows the wavelengths in vacuum.

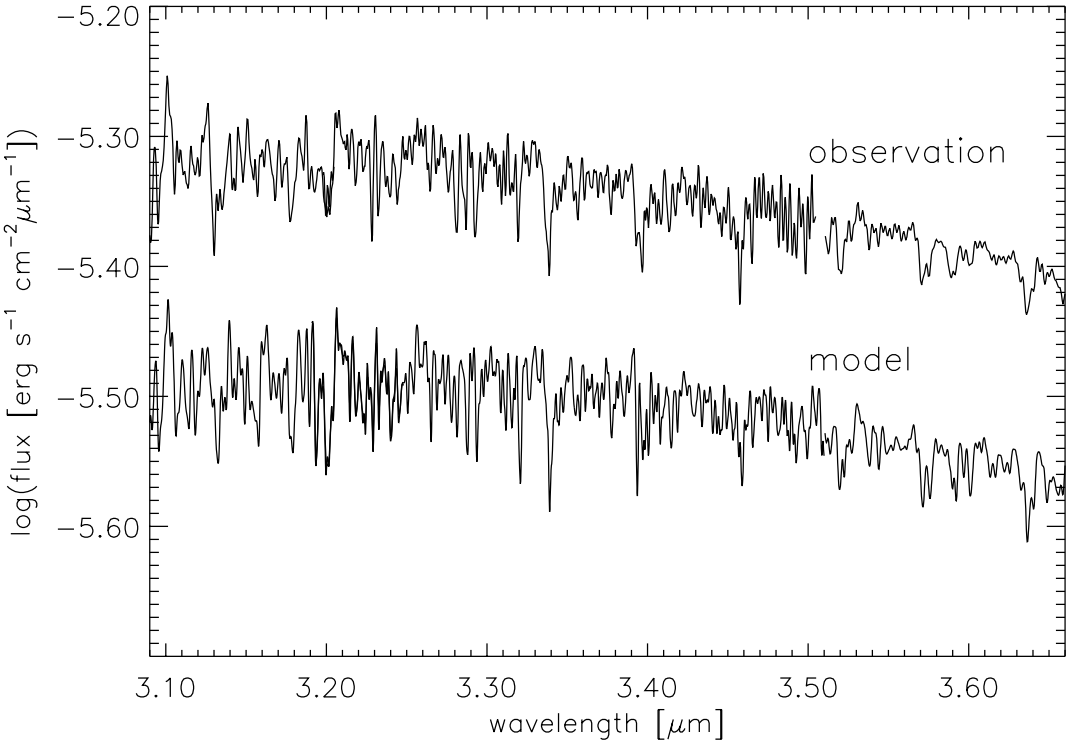

Fig. 2. The second half of the observed wavelength range of R Dor. The observations are shown above and the model spectrum is shifted down for clarity. The first half is shown in Fig. 1. The observed spectrum is a composite of several sub-spectra which sometimes overlap. However, at 3.51 μm there is a gap in the observations. The various observed bands have different spectral resolutions.

The continuous absorption as well as the new models will be fully described in a series of forth-coming papers in A&A (Gustafsson et al.; Jørgensen et al.; Plez et al., all in preparation). The new models were used by, among others, Decin et al. (2000) in their modeling of the K5III-giant α Tau.

Using the computed model photospheres we calculated synthetic spectra by solving the radiative transfer at a high wavelength resolution in a spherical geometry through the model photospheres. Using extensive line lists (consisting of wavelengths, excitation energies of the lower state of the transition, and line strengths in the form of oscillator strengths), we produce synthetic spectra of wavelength regions around the water vapour bands (ν_1 and ν_3) at 2.60–3.66 μm. The line lists included in the generation of the synthetic spectra are H_2O (Partridge & Schwenke 1997) (including all lines stronger than given by the condition $gf \times 10^{-\chi\theta} / \max(gf \times 10^{-\chi\theta}) > 10^{-5}$, where $\theta = 5040/3050$ and χ is the excitation energy in eV, leading to more than 2 million lines), CO (Goorvitch 1994), SiO (Langhoff & Bauschlicher 1993), CH (Jørgensen et al. 1996), CN (Jørgensen & Larsson 1990; Plez 1998, private communications), OH (Goldman et al. 1998), and C_2 (Querci et al. 1971; Jørgensen 2001, private communications). The accuracy and the completeness of these line lists are discussed in Decin (2000). We have also included CO_2 with data from the Hitran database (Rothman et al. 1987, 1992) and the Hitemp database (Rothman et al. in preparation).

In the generation of synthetic spectra, we calculate the radiative transfer for points in the spectrum separated by $\Delta\lambda \sim 1\,\mathrm{km\,s^{-1}}$ (corresponding to a resolution of $\lambda/\Delta\lambda \sim 330\,000$) even though the final resolution is much less. With a microturbulence of $\xi \sim 2\,\mathrm{km\,s^{-1}}$ in the model photosphere, this means that we are sure of sampling all lines in our database in the generation of the synthetic spectrum. This is an important point since a statistical approach, by only taking fewer, opacity-sampled points, will give an uncertainty in the synthesised spectrum. There will be noticeable differences in the synthesised spectra calculated with different sets of points, unless one chooses the spacing between the points smaller than the physical width of the line broadening. This is especially important when dealing with molecular bands, since the separation between lines differs greatly with wavelength depending on whether the lines are close to a band head or not. For example, by choosing random points in the spectrum, at which the radiative transfer is calculated for the synthetic spectrum, with a larger separation than we have chosen, one will tend to overestimate the absorption at band heads (or in regions with a high line density) and underestimate it far from band heads (or in regions with a low line density).

The emergent model spectra are subsequently convolved with a Gaussian in the same manner and with the same resolution as the observed bands. This will allow a comparison with ISO observations.

4. Procedure and results

In order to model the observations and to find a good fit, we have calculated a grid of synthetic spectra, allowing the effective temperature ($T_{\rm eff}$) and the surface gravity ($\log g$) of the models they are based on, to vary by increments of 50 K and 0.5 dex, respectively.

First, the over-all spectral shape was matched. This was done by convolving the observations and the models to a resolution of $R \sim 60$. The wavelength coverage of 2.6–3.7 μm is quite large and we find that especially the "low-frequency" spectral shape, in particular the slope, at 3.1–3.7 μm is sensitive to the effective temperature. This fact confines the possible range of effective temperatures. Subsequently, the molecular features, both their relative strengths and their amplitude are fitted visually. We find that we are able to fit our observations well, both the over-all shape and the molecular features, of the 3 μm region, for the phase at which the observations were made, with a synthetic spectrum based on a model photosphere of a temperature of 3000 K and a surface gravity of $\log g = 0$ (cgs), see Figs. 1 and 2. We point out that since the spectral region covered is sufficiently large we can fit both the general shape, or slope, of the spectrum as well as the molecular features themselves. However, we are not able to fit the flux level at the beginning of our observed region, at 2.6–3.8 μm. There is a discrepancy here and this will be discussed in Sect. 5. We also performed a more formal χ^2 fitting with the same result. We determined the correct multiplicative factor to multiply the modeled fluxes by (in order to account for the distance to the star), to be able to compare them with the observations, by minimising the χ^2 for every model in our grid. The parameters of the model giving the lowest overall χ^2 are also 3000 K and $\log g = 0$.

Actually, a synthetic spectrum calculated on the basis of a model photosphere with an effective temperature of 3100 K fits some of the molecular features of the observed range better (though only marginally) than does the 3000 K model, but this synthetic spectrum is then too steep in the long-wavelength region and the overall strength of the water bands is too weak, as is shown in Fig. 3. The uppermost spectrum in the figure shows the observations with the SWS01 observation as a back bone to outline the spectrum. The three spectra below are synthetic spectra based on model atmospheres of temperatures of 3100 K, 3000 K, and 2900 K. The low-resolution SWS01 observation is repeated for the three synthetic spectra. The overall shape of the hottest model is too steep, reflecting weaker water bands. The reverse is true for the coldest model. These facts may provide us with an estimate of the uncertainties in the temperature. Thus, with a conservative estimate of the uncertainties we arrive at a determination of the temperature of 3000 ± 100 K for R Doradus.

The surface gravity ($\log g$) is also a fundamental parameter, and is varied together with the effective temperature in the search for the best model, but the spectra are not as sensitive to this parameter as to the effective

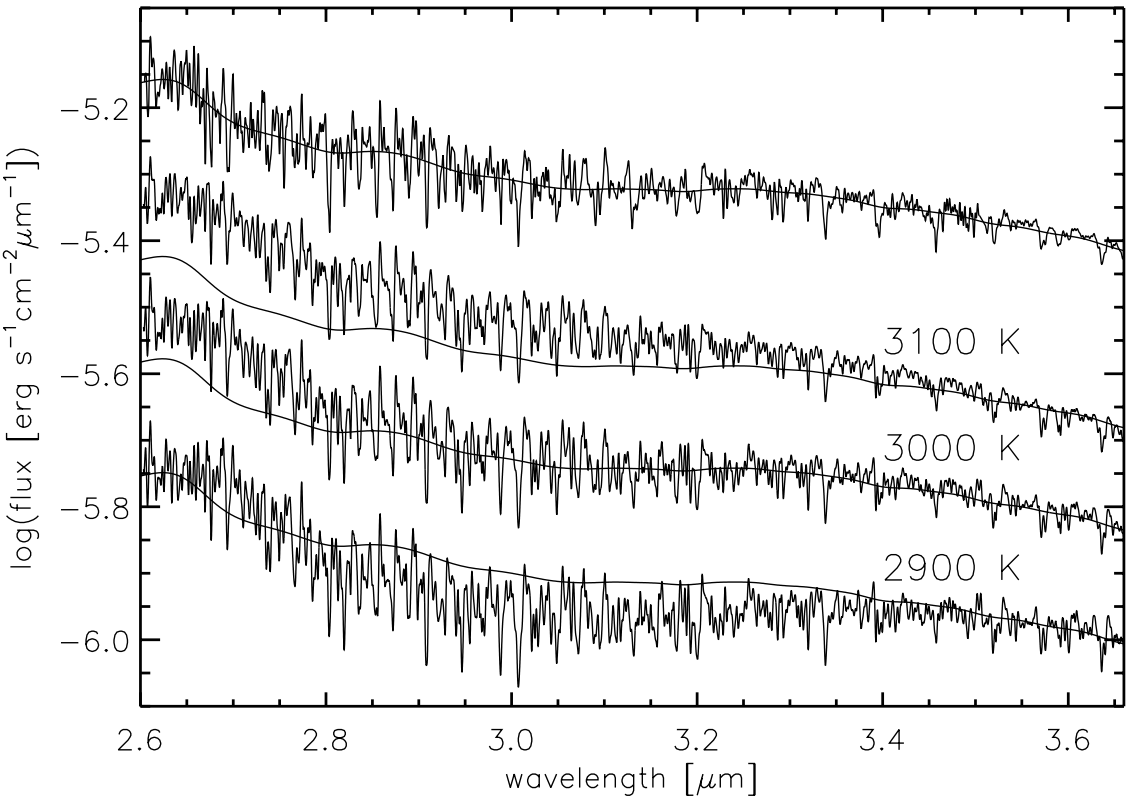

Fig. 3. The observed spectrum is shown uppermost, and below are shown three synthetic spectra generated from model atmospheres of temperatures of (from top to bottom) 3100 K, 3000 K, and 2900 K and of a surface gravity of $\log g = 0$. The SWS01 observation is shown to outline the observations and is repeated for the model spectra. These are arbitrarily normalised with the synthetic spectra at 3.5 μm.

temperature. For the grid of synthetic spectra that we have generated, we chose an increment of $\Delta \log g = 0.5$ (cgs). A change in surface gravity changes the relative strengths and details of the molecular features. We have chosen $\log g = 0$ as our best model but the uncertainty is quite large due to the low sensitivity of this parameter. Based on the fits, we estimate the limits of the surface gravity to be $\delta \log g = \pm 1$ (cgs). For a given surface gravity the stellar mass does not greatly change the spectral features or the spectral shape (typically by a few percent for a change in mass by a factor of 3).

Also, the metallicity of the star has an influence on the spectrum. This was also found by Decin et al. (2000) in their study of the red giant α Tau. We find that a decrease of the metallicity by 0.15 dex affects the absolute flux level and the relative slope of the spectrum but only beyond 3.3 μm. The molecular features hardly change. The slope of the spectrum is changed in such away that for a given effective temperature the slope decreases slightly for a lower metallicity.

In addition to the observed spectrum, Figs. 1 and 2 show our synthetic ones calculated with a hydrostatic model photosphere of an effective temperature of 3000 K and a surface gravity of $\log g = 0$. The stellar mass is assumed to be 1 solar mass and the chemical composition is assumed to be solar (Feast et al. 1999). For a metallicity of $[\mathrm{Fe/H}] = -0.15$ the temperature of the model that best fits the data is $T_{\mathrm{eff}} = 3050$ K. In the figures of the spectra, the fluxes are plotted on a logarithmic scale. The uncertainties in the absolute ISO fluxes originate from uncertainties in the gain factors of the different detectors (i.e. observed bands) and not from the levels of dark current of the bands. Allowing for these uncertainties and the distance to the star, which has to be taken into account when comparing stellar and model fluxes, the fluxes will differ only by a multiplicative factor. A plot of the logarithm of the fluxes allows a direct comparison with only an additive shift between them. The amplitude of the spectral features can be compared directly.

In Fig. 4, spectra including the contributions of only one molecule at a time, are shown. The relative importance of the H_2O, OH, CO, and SiO molecules contributing to the spectral features in the observed region is displayed. The total synthetic spectrum is also shown in the figure, and the SiO and the OH spectra are shifted for clarity. CO_2 does not contribute significantly; the two

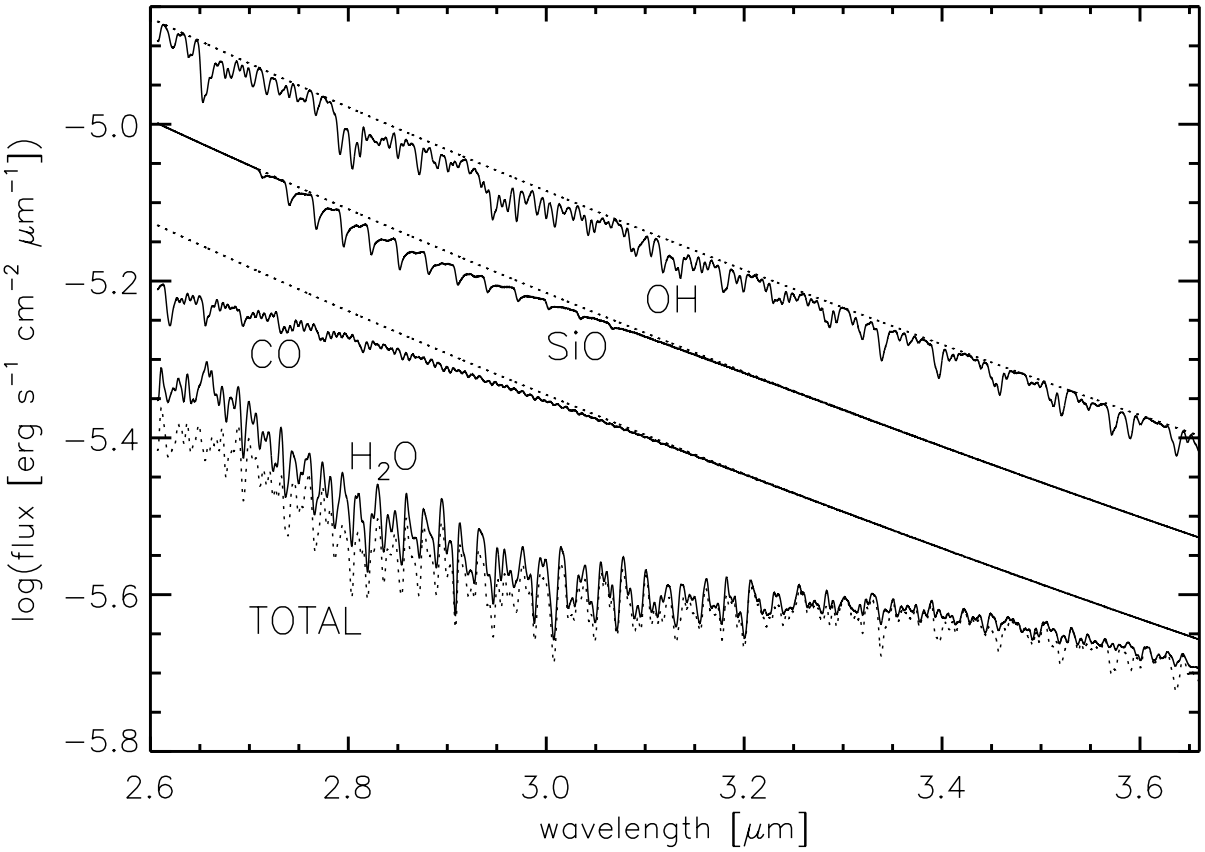

Fig. 4. The total spectrum and the spectra of the contributing molecules are shown convolved with a Gaussian profile of a width corresponding to 300 km s^{-1}. This is done to give a better overview. The SiO and OH spectra are shifted up for clarity. The dashed, straight line represents the continuum. The continuum is also shown for the shifted SiO and OH spectra.

vibration-rotational bands in this region are centered at 2.69 μm and 2.77 μm (Herzberg 1966), but these are only 2% deep as a maximum in our synthetic spectrum. The other molecules included in the spectral synthesis, i.e. CH, CN, and C_2, do not contribute to the spectrum at all. All spectra are convolved with a Gaussian profile with a width of 300 km s^{-1}, in order to provide a good overview of the spectrum. As can be seen, the main features are due to water vapour. It is the signatures of the $\Delta\nu_1 = 1$ and $\Delta\nu_3 = 1$ modes of the rotational-vibrational bands of H_2O. These modes are due to symmetric and antisymmetric stretching of the water molecule. The first overtone vibration-rotational band of the CO molecule starts contributing at 3.0 μm and increases toward shorter wavelengths. Several strong OH bands show their signatures in the synthesised spectrum including all molecules, especially at longer wavelengths (3.3–3.7 μm). These OH signatures can also be seen in the observed spectrum. The dashed line shows the continuum of the spectrum.

The partial pressure of water vapour in the model photosphere follows the gas pressure from the surface in to regions where the temperature has reached approximately 4000 K, with values of $P(H_2O)/P_g \sim 3 \times 10^{-3}$. Further in, the partial pressure of water vapour decreases rapidly due to the dissociation of the molecule.

5. Discussion

The physical structure of AGB stars are certainly variable to different extents. In order to model the atmospheres of these variable stars in a proper physical manner one needs to take the time dependence into account; this is increasingly important in the infrared wavelength range where the light originates from the outermost layers. The resulting dynamic effects could affect the density and temperature structures of the outer photosphere and therefore affect the line formation. For dynamic models of variable stars see, among others, Höfner & Dorfi (1997) and Bessell et al. (1996). The partial pressures of molecules in the outer photosphere may vary greatly over a pulsation period. However, the fact that R Dor shows only a modest variability of $\delta V \sim 1.5$ mag (the AAVSO International Database; J. A. Mattei 2001, private communication) suggests the feasibility of an attempt to model the stellar photosphere of this red giant with a hydrostatic model, as opposed to a dynamic model which takes into account time variations of the photospheric structure.

5.1. The hydrostatic modeling

In the hydrostatic modeling of M giants, there are several concerns to be addressed, which could potentially be

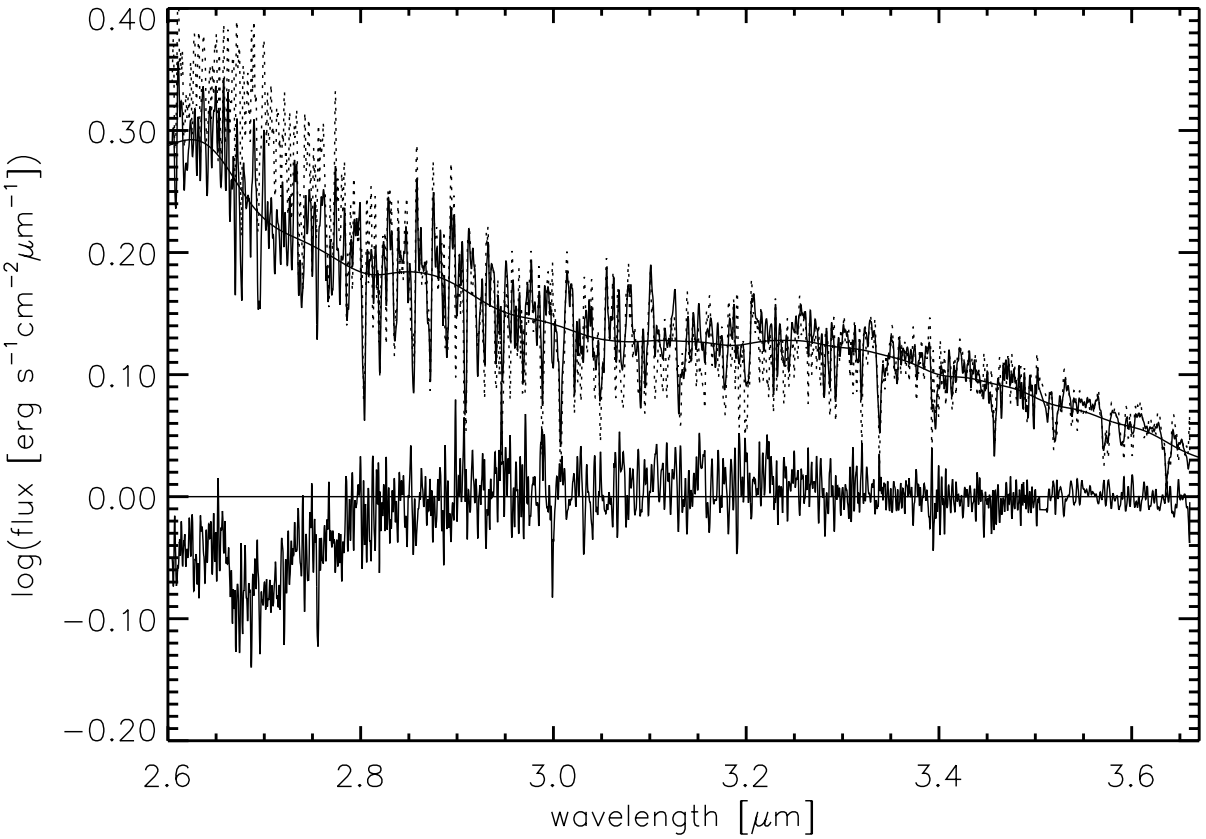

Fig. 5. The observed (upper, full line) and synthetic spectra (upper, dotted line) are compared directly. In order to outline all the observed, medium-resolution spectra (SWS06) the low-resolution ISO observation (SWS01) is also shown. This observation is convolved to a resolution of $\Delta\lambda = 0.05\,\mu$m. The lower spectrum shows the ratio of the observed and the modeled spectra. The ordinata is given in logarithmic flux units arbitrarily scaled.

important and explain discrepancies between observations and their modeling.

For example, the main source of continuous opacity in red giants in the IR spectral region is due to H^- free-free processes, a source of opacity that increases with wavelength. Therefore, IR lines are formed far out in the photosphere, where the assumptions made in the calculation of the model photosphere may be invalid. The outer atmospheres of M giants are very tenuous and the densities are low in the line-forming regions. One should therefore also be aware of the possibility of uncertainties due to NLTE effects affecting the lines.

Furthermore, the input data regarding molecular lines (line positions, excitation energies, and line strengths) and the completeness of the data, i.e. whether all relevant molecular bands are taken into account or not, are a concern. This is especially important for water vapour since it dominates the spectrum. Even bands far from the wavelength region considered, can contribute significantly to the synthetic spectrum through a large number of weak lines. Therefore, the inclusion of a relevant number of lines, including weak ones, is important (see also Jørgensen et al. 2001). Jones et al. (2002) discuss the completeness of the line list of water vapour by Partridge & Schwenke (1997), which is used here. They find a good match between their observations of M dwarfs and synthetic spectra based on the Partridge & Schwenke line list, indicating its relevance for studies of M stars.

Finally, the relative extension ($d = \Delta r_{\rm atm}/R_*$) of the photosphere, which is typically approximately 10%, means that sphericity effects could be important both in the calculation of the photospheric structure and in the radiative transfer, which generates a synthetic spectrum. Indeed, we calculate our model photospheres and synthetic spectra in spherical geometry as opposed to plane-parallel geometry normally used for dwarf-star models.

In spite of all the approximations made, the synthetic spectrum presented here reproduces the ISO-SWS observations reasonably well in the region of 2.8–3.66 μm, also keeping in mind the uncertainties in the observational data and in the reductions of the data. A direct comparison is presented in Fig. 5. The low-resolution SWS01 observation used to align the different medium-resolution SWS06 observations (see page 875) is also shown in the figure, as is the ratio of the observed and the modeled spectra. The negative spike in the ratio close to 3 μm probably shows an inaccuracy in the line list used. Thus, the use of a hydrostatic model photosphere for the synthesis of the

photospheric spectrum of this spectral region, seems to be quite adequate for the red, semi-regular variable R Doradus. This is certainly not the case for the more variable Mira stars (see for example Aringer et al. 2001).

5.2. The discrepancy at 2.6–2.8 μm

However, at the beginning of our interval, at 2.6–2.8 μm, we find a discrepancy of the over-all spectral shape, between our model and the ISO observations, see Fig. 5. We have not identified the cause of this, but we will discuss a few points in connection with this discrepancy, which reflect the approximations and shortcomings in the modeling.

First, the relevant absorption band of water vapour in the wavelength region we are considering here has its maximum at 2.65 μm (Jørgensen et al. 2001; Jones et al. 2002). Therefore, one would expect the lines at these wavelengths to be formed far out in the photosphere and one might be concerned as to whether the extension of the model photosphere is large enough to encompass this line-forming region properly. In our models the water vapour lines in the 2.6–2.8 μm region are indeed formed furthest out, with the strongest lines formed at an optical depth of approximately $\log \tau_{\rm Ross} = -4.8$ ($\log \tau_{\rm Ross}$ is the standard optical depth calculated by using the Rosseland mean extinction coefficient). However, our photospheric model is calculated out to $\log \tau_{\rm Ross} = -5.6$ which means that the strongest of the water vapour lines are formed within our photosphere and not on the outer boundary of the model. As a check, we also calculated a model extending to $\log \tau_{\rm Ross} = -6.2$, showing no noticeable differences in the calculated spectra. Still, the further out in the photosphere, the less likely are the assumptions made in the calculations valid. Thus, the discrepancy could have its origin in a too warm temperature structure in the outermost layers. Furthermore, the model is calculated in LTE and no line scattering is considered. Line scattering could yield a larger absorption in the water lines. Neither should one rule out dynamic effects here.

Second, some problems may exist concerning the input data; the line list calculations could be wrong just here, for instance due to missing bands, but this is not likely (see the discussion in Jones et al. 2002).

Third, there is certainly an extended atmosphere beyond the photosphere of AGB stars, which could affect their spectra in the infrared. The mass loss from the star creates a circumstellar envelope which can extend far out. Also, it is seen in dynamic model atmospheres of, for example, carbon-rich *Mira* stars, that the photospheres could extend far out due to pulsations and shocks (Höfner & Dorfi 1997). (These basic features of dynamic model photospheres are certainly valid also for oxygen-rich Mira stars.) Densities at a few stellar radii from the star can be an order of magnitude higher than the ones given by the equation of continuity in the stellar wind. Thus, the discrepancy could perhaps be explained by an additional absorption from an extended atmosphere. A discrepancy similar to the one we find between our modeled and observed spectra at 2.6–2.8 μm, was also found by Tsuji et al. (1997, 1998) in their analysis of the spectrum of the M 7 giant SW Vir. They attributed this to an excess absorption of warm water-vapour of non-photospheric origin. In order to explain several differences between models and infrared observations, Tsuji and collaborators (see for example Tsuji et al. 1997, 1998; Tsuji 2000a,b; Yamamura et al. 1999) have introduced the idea of a new, non-expanding, warm envelope situated further out than the photosphere but distinct from the cool, expanding circumstellar-envelope, at a distance of a few stellar radii from the star. The origin of the envelope is neither theoretically expected nor has it as yet received a theoretical explanation, but seems to be a common feature of M supergiants and M giants in general (Tsuji et al. 1998; Matsuura et al. 1999). This new envelope is shown to contain water vapour at temperatures of 1000–2000 K (Tsuji et al. 1997), resulting in non-photospheric signatures in IR spectra of M giants. This view was recently corroborated by ISO observations of the 6.3 μm bands of water vapour in early M giants, stars not expected to show signatures of water vapour (Tsuji 2001). Thus, the discrepancy between our modeled and observed spectra at 2.6–2.8 μm could be a result of an extra absorption component due to a non-expanding, warm envelope. We are in the process of modeling such a region (Ryde et al. in preparation). It is tempting to suggest in this scenario, that a star with a sufficiently low mass-loss rate will not be able to accelerate a wind from the stellar surface to velocities above the velocity of escape, but instead accumulates material "close" to the star where it could form a relatively dense, warm layer including H_2O.

5.3. The derived effective temperature of R Dor

Our derived effective temperature of 3000 ± 100 K, which is based on the ISO spectrum of the 2.60–3.66 μm region, is somewhat higher than values found in the literature. For example, Bedding et al. (1997) estimate an effective temperature of 2740 ± 190 K from measurements of the angular diameter and the apparent flux of R Doradus. As is discussed by these authors, other indirect estimates of the effective temperature in the literature yield even lower temperatures. We note that, given the inferred radius of $R = 370 \pm 50\,R_\odot$ of Bedding et al. (1997), our temperature would yield a luminosity more characteristic of a supergiant. However, we also note that Fluks et al. (1994), who derive effective temperatures for all M-spectral subtypes of the MK classification based on spectroscopic observations of M giants in the solar neighbourhood, find an $T_{\rm eff} = 3126$ K for the M7 class. They classify R Dor as an M7 giant and they derive an effective temperature of 2890 K for the M8 class.

Several possible reasons exist for the slightly higher temperature deduced in this paper as compared to most

of the literature values. First, as was pointed out by Bedding et al. (1997), there may be inadequacies in indirect methods of determining effective temperatures from the colours of red stars. Second, Jones et al. (2002), in their fit of ISO spectra of M *dwarfs* with synthetic spectra based on the line list of Partridge & Schwenke (1997), also find effective temperatures systematically higher than those found in the literature, which are obviously based on several different methods. They suggest that an explanation of this could be the non-physical line splittings of the Partridge & Schwenke (1997) line list, which lead to too strong water vapour transitions for a given temperature. This would lead to a slightly higher effective temperature for a synthetic fit of a stellar spectrum. Third, R Dor is intrinsically variable, albeit with a small amplitude. As has been discussed in, for example, Aringer (2000), low-resolution ISO-SWS spectra of oxygen-rich, semi-regular variables on the AGB can be modeled with a sequence of hydrostatic models of different effective temperatures over the period of the star. Thus, one would indeed expect slightly different effective temperatures to be determined at different phases of the pulsation.

6. Conclusion

We have attempted to synthesis an observed spectral region, covering 1.06 μm of the spectrum around 3 μm of the red giant R Doradus at a spectral resolution of $R \sim 2000$–2500. The synthesised spectrum is based on a MARCS hydrostatic model-photosphere. We are successful in reproducing the 2.80–3.66 μm region, but encounter a discrepancy in the beginning of the spectral region of our observations; $\sim$2.6–2.8 μm. We have discussed possible explanations of this discrepancy, but have not identified the cause.

The good agreement with the medium-resolution ISO-SWS06 observations, apart from the region with the strongest water bands, suggests the adequacy of using a hydrostatic model photosphere for this particular star, and the completeness and correctness of our input data in the form of the molecular opacity for the calculation of the spectrum. Given all the possible failures of the model to correctly describe the physical picture of the outer photospheres of red giants, the agreement is promising. It shows once again the accuracy and the strength of the new MARCS code also in the infrared wavelength region. Thus, the modeling of moderately varying red giants, such as semi-regular variables, in the near-infrared region with hydrostatic model photospheres may be a reasonable approximation. Note, however, that for the very variable Mira stars in general, hydrostatic model atmospheres certainly fail to reproduce observed spectra (see, for example, Aringer et al. 2001). Attention should also always be given to the extended atmospheres of these stars, which could affect the spectra and especially so in the infrared wavelength region. This extended atmosphere is a possible reason for the discrepancy in the 2.6–2.8 μm region.

The spectral signatures in the spectrum presented here are mostly due to photospheric water vapour but several photospheric CO and OH bands are also identified. The spectral region is found to be very temperature sensitive, leading us to an estimate of the effective temperature of the star of (3000 ± 100) K. The best-fit synthetic spectrum was based on a model photosphere of a surface gravity of $\log g = 0 \pm 1$ (cgs). The temperature found here is slightly higher than the ones reported in the literature. A possible reason for this is a problem with the water vapour line list of Partridge & Schwenke (1997), as suggested by Jones et al. (2002).

Acknowledgements. We should like to thank Professors Bengt Gustafsson and David L. Lambert for inspiration and enlightening discussions and the referee for valuable comments and suggestions. This work was supported by the P. E. Lindahl Foundation Fund of the Royal Swedish Academy of Sciences and the Swedish Foundation for International Cooperation in Research and Higher Education.

References

Aringer, B. 2000, Ph.D. Thesis, Univ. Vienna
Aringer, B., Jørgensen, U. G., Kerschbaum, F., Hron, J., & Höfner, S. 2001, IAU Coll., 185, ed. C. Aerts, T. Bedding, & J. Christensen-Dansgaard, in press
Bedding, T. R., Zijlstra, A. A., Jones, A., & Foster, G. 1998, MNRAS, 301, 1073
Bedding, T. R., Zijlstra, A. A., von der Luhe, O., et al. 1997, MNRAS, 286, 957
Bessell, M., Scholz, M., & Wood, P. 1996, A&A, 307, 481
de Graauw, T., Haser, L. N., Beintema, D. A., et al. 1996, A&A, 315, L49
de Graauw, T., van den Ancker, M., Bauer, O., et al. 2000, The ISO Handbook, volume VI: SWS–the Short Wavelength Spectrometer, `www.iso.vilspa.esa.es/manuals/HANDBOOK/VI/ sws_hb/`
Decin, L. 2000, Ph.D. Thesis, University of Leuven
Decin, L., Waelkens, C., Eriksson, K., et al. 2000, A&A, 364, 137
Edvardsson, B., Andersen, J., Gustafsson, B., et al. 1993, A&A, 275, 101
Feast, M., & Whitelock, P. 1999, in The Evolution of the Milky Way: stars versus clusters, ed. F. Matteucci, & F. Giovannelli (Kluwer Academic Publishers), 229
Fluks, M. A., Plez, B., The, P. S., et al. 1994, A&AS, 105, 311
Goldman, A., Schoenfeld, W., Goorvitch, D., et al. 1998, JQSRT, 59, 453
Goorvitch, D. 1994, ApJS, 95, 535
Gustafsson, B., Bell, R. A., Eriksson, K., & Nordlund, Å. 1975, A&A, 42, 407
Gustafsson, B., & Ryde, N. 2000, in IAU Symp., 177, 481
Habing, H. J. 1996, A&ARv, 7, 97
Herzberg, G. 1966, Molecular Spectra and Molecular Structure, vol. II (Krieger Publishing Company, Malabar, Florida)
Höfner, S., & Dorfi, E. A. 1997, A&A, 319, 648
Jones, H. R. A., Pavlenko, Y., Viti, S., & Tennyson, J. 2002, MNRAS, 330, 675

Jørgensen, U. G., Jensen, P., Sørensen, G. O., & Aringer, B. 2001, A&A, 372, 249
Jørgensen, U. G., Johnson, H. R., & Nordlund, Å. 1992, A&A, 261, 263
Jørgensen, U. G., & Larsson, M. 1990, A&A, 238, 424
Jørgensen, U. G., Larsson, M., Iwamae, A., & Yu, B. 1996, A&A, 315, 204
Kerschbaum, F., & Hron, J. 1992, A&A, 263, 97
Kessler, M. F., Steinz, J. A., Anderegg, M. E., et al. 1996, A&A, 315, L27
Kholopov, P. N. 1988, General Catalogue of Variable Stars, 4th ed., Bull. Inf. Centre Données Stellaires
Langhoff, S. R., & Bauschlicher, C. W. 1993, Chem. Phys. Lett., 211, 305
Lebzelter, T., & Hron, J. 1999, A&A, 351, 533
Loup, C., Forveille, T., Omont, A., & Paul, J. F. 1993, A&AS, 99, 291
Markwick, A. J., & Millar, T. J. 2000, A&A, 359, 1162
Matsuura, M., Yamamura, I., Murakami, H., Freund, M. M., & Tanaka, M. 1999, A&A, 348, 579
Olofsson, H. 1996, Ap&SS, 245, 169
Partridge, H., & Schwenke, D. 1997, J. Chem. Phys., 106, 4618
Piskunov, N. E., Kupka, F., Ryabchikova, T. A., Weiss, W. W., & Jeffery, C. S. 1995, A&AS, 112, 525
Plez, B., Brett, J. M., & Nordlund, Å. 1992, A&A, 256, 551
Querci, F., Querci, M., & Kunde, V. 1971, A&A, 15, 256
Rothman, L., Gamache, R., Goldman, A., et al. 1987, Appl. Opt., 26(19), 4058
Rothman, L., Gamache, R., Tipping, R. H., et al. 1992, JQSRT, 48(5), 469
Ryde, N., Eriksson, K., & Gustafsson, B. 1999, A&A, 341, 579
Ryde, N., Eriksson, K., Gustafsson, B., Olofsson, H., & Plez, B. 1998, in IAU Symp., 191
Tsuji, T. 2000a, ApJ, 540, L99
Tsuji, T. 2000b, ApJ, 538, 801
Tsuji, T. 2001, A&A, 376, L1
Tsuji, T., Ohnaka, K., Aoki, W., & Yamamura, I. 1997, A&A, 320, L1
Tsuji, T., Ohnaka, K., Aoki, W., & Yamamura, I. 1998, Ap&SS, 255, 293
Yamamura, I., de Jong, T., & Cami, J. 1999, A&A, 348, L55